

# Kent Academic Repository

## Full text document (pdf)

### Citation for published version

Sarell, CJ and Karamanos, TK and White, SJ and Bunka, DH and Kalverda, AP and Thompson, GS and Barker, AM and Stockley, PG and Radford, SE (2014) Distinguishing closely related amyloid precursors using an RNA aptamer. *The Journal of Biological Chemistry*, 289 . pp. 26859-26871. ISSN 0021-9258.

### DOI

<https://doi.org/10.1074/jbc.M114.595066>

### Link to record in KAR

<https://kar.kent.ac.uk/71801/>

### Document Version

Publisher pdf

#### Copyright & reuse

Content in the Kent Academic Repository is made available for research purposes. Unless otherwise stated all content is protected by copyright and in the absence of an open licence (eg Creative Commons), permissions for further reuse of content should be sought from the publisher, author or other copyright holder.

#### Versions of research

The version in the Kent Academic Repository may differ from the final published version.

Users are advised to check <http://kar.kent.ac.uk> for the status of the paper. **Users should always cite the published version of record.**

#### Enquiries

For any further enquiries regarding the licence status of this document, please contact:

[researchsupport@kent.ac.uk](mailto:researchsupport@kent.ac.uk)

If you believe this document infringes copyright then please contact the KAR admin team with the take-down information provided at <http://kar.kent.ac.uk/contact.html>

## Distinguishing closely-related amyloid precursors using an RNA aptamer

Claire J. Sarell<sup>§</sup>, Theodoros K. Karamanos, Simon J. White, David H. J. Bunka<sup>†</sup>, Arnout P. Kalverda, Gary S. Thompson, Amy M. Barker, Peter G. Stockley<sup>1</sup> & Sheena E. Radford<sup>1</sup>

Astbury Centre for Structural Molecular Biology and School of Molecular and Cellular Biology, University of Leeds, Leeds LS2 9JT, United Kingdom

Running title: *Amyloid precursors and RNA aptamers*

<sup>1</sup>Corresponding authors: Astbury Centre for Structural Molecular Biology and School of Molecular and Cellular Biology, University of Leeds, LS2 9JT, UK.  
Tel: (SER) +44(0) 113 343 3170; (PGS) +44(0) 113 343 3092; E-mail: [s.e.radford@leeds.ac.uk](mailto:s.e.radford@leeds.ac.uk) or [p.g.stockley@leeds.ac.uk](mailto:p.g.stockley@leeds.ac.uk)

### Current address:

<sup>†</sup>Aptamer group, Suite 2.80 - 2.87, Bio Centre, Innovation Way, Heslington, York, YO10 5NY

<sup>§</sup> Medical Research Council Prion Unit, Department of Neurodegenerative Disease, University College London, Institute of Neurology, Queen Square, London WC1N 3BG

### Abbreviations

h $\beta_2$ m, human  $\beta_2$ -microglobulin; TEM, transmission electron microscopy; LS, long-straight  $\beta_2$ m fibrils; afu, arbitrary fluorescence units; RMSD, root-mean-square deviation; SELEX, Systematic Evolution of Ligands by Exponential Enrichment.

**Keywords:** RNA aptamer,  $\beta_2$ -microglobulin, amyloid fibril, co-polymerization, amyloid precursor, specificity

**CAPSULE**

**Background:** Altering the co-polymerization of proteins into amyloid fibrils provides an opportunity for manipulating fibril assembly

**Results:** NMR and kinetic analysis showed that an RNA aptamer distinguishes between two highly similar co-aggregating proteins

**Conclusion:** RNA aptamers are specific and discriminatory probes able to modulate amyloid formation

**Significance:** Aptamers can be used as tools to differentiate amyloid precursors that are closely related and alter assembly

**ABSTRACT**

Whilst amyloid fibrils assembled *in vitro* commonly involve a single protein, fibrils formed *in vivo* can contain multiple protein sequences. The amyloidogenic protein human  $\beta_2$ -microglobulin ( $h\beta_2m$ ) can co-polymerize with its N-terminally truncated variant ( $\Delta N6$ ) *in vitro* to form hetero-polymeric fibrils that differ from their homo-polymeric counterparts. Discrimination between the different assembly precursors; for example by binding of a biomolecule to one species in a mixture of conformers, offers an opportunity to alter the course of co-assembly and the properties of the fibrils formed. Here, using  $h\beta_2m$  and its amyloidogenic counterpart,  $\Delta N6$ , we describe selection of a 2'F-modified RNA aptamer able to distinguish between these very similar proteins. SELEX with a N30 RNA pool yielded an aptamer (B6) that binds  $h\beta_2m$  with an  $EC_{50}$  of  $\sim 200$  nM. NMR spectroscopy was used to assign the  $^1H$ - $^{15}N$  HSQC spectrum of the B6- $h\beta_2m$  complex, revealing that the aptamer binds to the face of  $h\beta_2m$  containing the A, B, E and D  $\beta$ -strands. By contrast, binding of B6 to  $\Delta N6$  is weak and less specific. Kinetic analysis of the effect of B6 on co-polymerization of  $h\beta_2m$  and  $\Delta N6$  revealed that the aptamer alters the kinetics of co-polymerization of the two proteins. The results reveal the potential of RNA aptamers as tools for elucidating the mechanisms of co-assembly in amyloid formation and as reagents able to discriminate between very similar protein conformers with different amyloid propensity.

**INTRODUCTION**

Despite the array of different proteins and peptides with distinct amino acid sequences that are known to be able to assemble into amyloid fibrils *in vitro* and/or *in vivo* (1), the precise molecular mechanism(s) by which these different proteins/peptides self-assemble into amyloid fibrils, and how the assembly process results in disease remain unclear (2). Amyloid formation commences with the generation of aggregation-prone monomeric precursors. These species can be unfolded/disordered, partially structured or even native-like (3) and their structural properties, even though potentially similar to their non-amyloidogenic counterparts, dictate the fate of amyloid assembly (4). This is exemplified by the observation that the same amino acid sequence can form conformationally distinct amyloid structures *in vitro* by varying the temperature, altering the agitation conditions, adding co-solvents, metal ions or other molecules, or even changing the surface properties of the incubation vessel (reviewed in (5)). An extra level of complexity is added by the ability of different protein/peptide precursors to co-polymerize, resulting in new fibril polymorphs with different amyloid architectures, stabilities and/or different kinetics of assembly than those formed by each protein alone (4, 6, 7). Indeed, there are multiple examples of amyloidogenic proteins that are able to co-polymerize, such as islet amyloid polypeptide (IAPP) and  $A\beta$  (6, 8), tau and  $\alpha$ -synuclein (9) and insulin and transthyretin (10). Although the importance of identifying and characterizing rarely-populated amyloidogenic precursors is widely appreciated (3), this remains a significant challenge because of the transient nature and heterogeneity of assembly intermediates (11). The development of reagents able to discriminate aggregation-prone species among a pool of structurally similar molecules is crucial to deciphering the mechanisms of protein assembly into amyloid and to inform the design of therapeutic/diagnostic strategies able to target individual amyloid precursors (12).

Human  $\beta_2$ -microglobulin ( $h\beta_2m$ ) is a small protein that forms amyloid deposits in collagen-rich osteoarticular sites, resulting in the disorder dialysis-related amyloidosis (DRA) (13, 14). Despite the propensity of  $h\beta_2m$  to form amyloid fibrils *in vivo*, conditions that destabilize the native

structure of  $h\beta_2m$  such as low pH (15), the presence of SDS (16), or other co-solvents or metal ions (17, 18), are required for fibril formation on an experimentally tractable timescale *in vitro*. Removal of the N-terminal six residues from  $h\beta_2m$  (the sequence IQRTPK), creating the variant  $\Delta N6$ , disrupts the thermodynamic and kinetic stability of  $h\beta_2m$  and, as a result,  $\Delta N6$  can self-assemble into amyloid fibrils rapidly and spontaneously without the need to add detergents, metal ions or other reagents (19, 20).  $\Delta N6$  retains a native-like structure, displaying a backbone RMSD of only  $\sim 1.5$  Å compared with  $h\beta_2m$  (19), and contains a non-native *trans* X-Pro32 (Figures 1A, B) which has been shown to be vital for fibril formation (21, 22). Isomerization of the X-Pro32 bond results in structural reorganization of the side chains in the apical region of  $h\beta_2m$  resulting in a protein with different surface hydrophobicity and electrostatic properties (19). Crucially,  $\Delta N6$  can promote the aggregation of  $h\beta_2m$  even when added in trace amounts (19), resulting in co-polymerization of both proteins into heteropolymeric amyloid fibrils (4). This interaction allows amyloid formation of  $h\beta_2m$  to be investigated in the absence of additives at physiologically relevant pH values (4).

The design of molecules able to bind  $h\beta_2m$  or its amyloidogenic counterpart,  $\Delta N6$ , would offer an opportunity to increase understanding of the interaction between these co-assembling monomers and explore the aggregation pathway that leads to their co-polymerization into amyloid fibrils. However, such a task is hindered by the high sequence and structural homology (Figure 1A) of the two proteins and their dynamic nature (19). In this study, we used *in vitro* selection to identify an RNA aptamer able to bind  $h\beta_2m$  preferentially to  $\Delta N6$  and to alter fibril co-assembly. Nucleic acid aptamer selection has been used previously to generate RNA aptamers able to discriminate monomeric PrP<sup>SC</sup> and recombinant PrP<sup>C</sup> (23, 24), and to bind to A $\beta$  monomers rather than fibrils (25-27). Oligomers of amyloidogenic proteins have also been used as targets: DNA/RNA aptamers have been raised against oligomers of  $\alpha$ -synuclein (28) and A $\beta$ 40 (29) respectively.

Previously, we used SELEX to isolate RNA aptamers against fibrillar  $h\beta_2m$  that were counter-selected against the low pH, partially unfolded,

$h\beta_2m$  monomer from which these fibrils were formed (30). Here, we extend this approach using SELEX to isolate 2'-fluoro-modified RNA aptamers against native monomeric  $h\beta_2m$ . The selected aptamer discriminates in its binding to  $h\beta_2m$  or  $\Delta N6$  at pH 6.2, conditions in which both proteins are folded, but only  $\Delta N6$  is able to assemble spontaneously into amyloid fibrils (19). The  $h\beta_2m$  specific aptamer was minimized to a 44 nucleotide long fragment and its binding interface, affinity and specificity for  $h\beta_2m$  determined. The aptamer binds tightly and specifically to the  $\beta$ -sheet of  $h\beta_2m$  containing the A, B, E, D  $\beta$ -strands, but only weakly and less specifically to  $\Delta N6$ . Addition of the aptamer to a mixture of  $h\beta_2m$  and  $\Delta N6$  under conditions (pH 6.2) that promote co-assembly (4) disfavors the interaction between the two proteins early in assembly, making  $h\beta_2m$  to remain soluble for longer. The results reveal the ability of RNA aptamers to discriminate and bind to a specific protein conformer within a complex mixture of structurally similar co-polymerizing species, altering the course of amyloid assembly.

## EXPERIMENTAL PROCEDURES

*Protein preparation* -  $h\beta_2m$  and  $\Delta N6$  were expressed and purified as previously described (19). For NMR experiments <sup>15</sup>N and <sup>13</sup>C labeled  $h\beta_2m$  and  $\Delta N6$  were prepared as described in (31).

*Biotinylation and immobilization of  $h\beta_2m$*  - Monomeric  $h\beta_2m$  ( $\sim 1$  mg) was biotinylated (EZLink™ Sulfo-NHS-LC-LC-biotin, Pierce Biotechnologies) at pH 7 using a 20-fold molar excess of biotin over the total protein concentration, according to the manufacturer's protocol. The biotinylated monomer was then immobilized on 1  $\mu$ m streptavidin-coated microspheres (Dynabeads™, Life Technologies) using the manufacturer's protocol.

*In vitro selection* - A Biomek 2000 laboratory automation work station (Beckman Coulter) was used to perform 12 rounds of *in vitro* selections with an N30 library of 2'-F-modified pyrimidine RNA, encompassing  $\sim 10^{15}$  potential sequences, and transcribed using the Y639F/H784A variant of T7 RNA polymerase (32), using minor modifications of the protocols described previously (30). Selections were carried out in 50 mM MES buffer containing 120 mM NaCl, pH

6.2. Negative selections were carried out at each round of SELEX using streptavidin Dynabeads coated with Tris-inactivated linker. Stringency was increased after round 5 by decreasing the number of beads containing monomeric  $h\beta_2m$  by half and increasing the number of washes from 10 to 13. The reverse transcriptase-PCR products were analyzed by native PAGE after each group of 5 rounds of selection to confirm the isolation of products for the next round of selection. Individual aptamer clones were produced by *in vitro* transcription using 10 mM final concentrations of each nucleotide triphosphate using 2'F CTP and 2'F UTP for production of modified RNAs. RNA concentrations were determined using the following extinction coefficients: B6 -  $1026.3 \text{ mM}^{-1} \text{ cm}^{-1}$ ; B6 minimised (B6min) -  $553.2 \text{ mM}^{-1} \text{ cm}^{-1}$  and B9 -  $1054.2 \text{ mM}^{-1} \text{ cm}^{-1}$ .

*Synthesis of minimised B6 - B6min* (5'-GGG AAU UCU GAG CUA CUC CCU UUU GGG CCC GGC UAU GAU UCC CG-3') was synthesized with and without 2'F-modified pyrimidine nucleotides (named 2'F B6min and 2'OH B6min, respectively) on an ABI 394 RNA synthesiser at a 1  $\mu\text{M}$  scale using the protocols described previously (33). The phosphoramidites used for synthesis of 2'F B6min were as follows: *N*-benzoyl-protected adenosine, *N*-dimethylformamidinyl-protected guanosine (dmf-rG), *N*-acetyl-protected-2'-fluoro deoxycytidine and 2'-fluoro-deoxyuridine. For synthesis of 2'OH B6min *N*-acetyl-protected-2'-fluoro deoxycytidine and 2'-fluoro-deoxyuridine were replaced with *N*-acetyl-protected-cytidine and uridine phosphoramidites (Link Technologies Ltd.). Cyanoethyl-(*N,N'*-diisopropyl) and *t*-butyldimethylsilyl (TBDMS) groups were present on the 3' and 2' hydroxyl groups. Treatment with ammonia-saturated methanol at room temperature for 24 h was used to remove protecting groups and to cleave RNA from controlled-pore glass (CPG) resin. Methanol was removed under vacuum and the RNA pellet re-suspended in anhydrous DMSO. One volume of triethylamine trihydrofluoride was added and incubated at room temperature to remove TBDMS, the deprotected RNA was precipitated with butan-1-ol and resuspended in diethylpyrocarbonate-treated water (Severn Biotech) before being purified by reverse-phase HPLC at 55 °C (34). RNA fractions were collected, lyophilized and desalted into 18.2 m $\Omega$  H<sub>2</sub>O. The RNA was analyzed on a 10% (w/v)

denaturing polyacrylamide urea gel stained with ethidium bromide. The RNA was synthesized using dmf-rG CPG to avoid incorporation of a pyrimidine with a ribose sugar at the 3' end. This additional guanosine has no effect on the secondary structure of 2'F B6min or 2'OH B6min as predicted by Mfold (35).

*Surface Plasmon Resonance (SPR)* - A BIAcore3000 instrument was used with a streptavidin-coated gold sensorchip (BIAcore SA chip). A flow-rate of 10  $\mu\text{l min}^{-1}$  was used with a running buffer of 50 mM MES, 120 mM NaCl, pH 6.2. 50  $\mu\text{l}$  of 50  $\mu\text{g ml}^{-1}$  of biotinylated monomer was injected over separate flow-cells so that ~200 RU of protein was immobilized. RNAs were dialyzed into running buffer before injection across the surface to minimize bulk refractive index effects. Flow-cells were regenerated using a 20  $\mu\text{l}$  wash of 5 M NaCl. All sensorgrams were corrected by subtracting the signals of an equivalent injection across an underivatized flow-cell. Data were analyzed using the manufacturer's software (BIAevaluation).

*Intrinsic fluorescence quenching* - The fluorescence of tryptophan residues in 1  $\mu\text{M}$   $h\beta_2m$  or  $\Delta\text{N6}$  was excited at 290 nm and fluorescence emission was measured between 300 and 390 nm in the presence of increasing concentrations of 2'F B6min or 2'OH B6min in 50 mM MES buffer containing 120 mM NaCl pH 6.2 at 25 °C. Due to the large extinction coefficient of the RNA aptamer at 260 nm ( $553.2 \text{ mM}^{-1} \text{ cm}^{-1}$ ) the absorbance of the  $h\beta_2m$ /aptamer solution at 290 nm was measured after each addition of aptamer to ensure that the absorbance of the solution was below 0.05 au at 290 nm so that inner filter effects do not contribute to the data (36). Fluorescence emission was measured using a Photon Technology International QM-1 spectrofluorimeter (PTI) using 10 nm slit-widths. The data for binding of 2'F B6min to  $h\beta_2m$  were normalized to a value of 0 in the absence of aptamer and a fluorescence signal of 1 obtained upon saturation. The data were then fitted to the following logistic equation to extract the half maximal effective concentration ( $EC_{50}$ ) using in-house scripts:

$$f(x) = \min + \frac{\max - \min}{1 + \left(x/EC_{50}\right)^{-Hill}}$$



where  $max$ ,  $min$  represents the maximum and minimum fluorescence signals,  $Hill$  is the Hill coefficient,  $f(x)$  is the fluorescence units and  $x$  is the concentration of the aptamer in nM. For 2'F B6min to  $\Delta N6$  and 2'OH B6min to  $h\beta_2m$  no change in fluorescence was observed over the concentration range studied.

**NMR spectroscopy** - Samples of  $^{13}C$ - $^{15}N$ -labeled protein (60  $\mu M$ ) in 50 mM MES buffer containing 120 mM NaCl, pH 6.2, 0.02% (w/v) sodium azide, 0.1 mM EDTA, 90% (v/v)  $H_2O$ /10% (v/v)  $D_2O$  were used for NMR experiments. Synthetic 2'F B6min or 2'OH B6min was added into the protein solution from a concentrated stock (typically 200  $\mu M$ ). Working at a concentration of 60  $\mu M$  necessitated the use of a sensitivity optimized strategy for obtaining assignments. This was achieved using a reduced dimensionality approach based on Hadamard encoding (37). Sequential assignments were obtained from analysis of Hadamard encoded 2D H(N- $H_2$ ) CA and H(N- $H_2$ )(CO)CA experiments where a 2 step Hadamard matrix is introduced on  $^{15}N$  to subdivide the peaks into two subspectra where most signals can be addressed from their  $^1H$  shift alone and the dimensionality can be reduced to 2 to maximize sensitivity. Spectra were recorded at 25  $^\circ C$  on a Varian Inova 750 MHz spectrometer equipped with a cryogenic probe and were processed using NMRPipe and analyzed using CCPN analysis (38). To calculate the intensity profiles shown in Figure 7, peak intensities were normalized to the number of scans and the protein concentration used for each experiment. Intensity profiles were calculated as the ratio of the normalized peak intensity of each resonance in the apo spectrum ( $I_0$ ) versus the normalized intensity at the same position but in the aptamer-bound spectrum ( $I$ ). Therefore, the loss of native signal plotted in Figure 7 does not require full assignment of the aptamer-bound spectrum.

**Assembly of amyloid fibrils** - 40  $\mu M$   $h\beta_2m$  and 40  $\mu M$   $\Delta N6$  in the presence or absence of two molar equivalents of 2'F B6min were co-incubated in 50 mM MES buffer containing 120 mM NaCl, pH 6.2, 0.02% (w/w) sodium azide at 600 rpm, 37  $^\circ C$  in a Thriller Thermoshaker incubator (Peqlab). Each sample (100  $\mu l$ ) was incubated in 0.5 ml plastic Eppendorf tubes. Aliquots of 8  $\mu l$  were removed at different time points during incubation and immediately centrifuged at 14,000 g for 20

min. The supernatant was separated from the pellet and both supernatant and pellet were frozen at -20  $^\circ C$  for subsequent analysis by SDS-PAGE.

**SDS-PAGE** - The effect of 2'F B6min on fibril formation was monitored using 15% polyacrylamide Tris-Tricine gels. Samples of the supernatant and pellet were thawed and the pellet resuspended in 8  $\mu l$  of 50 mM MES buffer containing 120 mM NaCl, pH 6.2. Both the supernatant and resuspended pellet were added 1:1 to loading buffer (50 mM Tris-HCl, pH 6.8, 100 mM DTT, 2% (w/v) SDS, 0.1% (w/v) bromophenol blue, 10% (v/v) glycerol) and boiled for 5 min before loading 15  $\mu l$  into the gel. Gels were stained with Coomassie Instant Blue (Expedeon) and imaged by SnapGene software (Syngene).

**Electron microscopy** - At the end of fibril assembly, 10  $\mu l$  of sample were applied to a carbon-coated grid. The grid was then carefully dried with filter paper before it was negatively stained by the addition of 10  $\mu l$  of 4% (w/v) uranyl acetate as described in (39). Micrographs were recorded on a Philips CM10 or a JEOL JEM-1400 electron microscope.

## RESULTS-

### *Selection of $h\beta_2m$ -specific 2'F-RNA aptamers*

Co-incubation of  $\Delta N6$  and  $h\beta_2m$  results in the two proteins polymerizing into hetero-polymeric amyloid-like fibrils that are morphologically and thermodynamically distinct compared with fibrils formed by  $\Delta N6$  or  $h\beta_2m$  alone (4). In order to control the co-assembly of these proteins we attempted to select RNA aptamers capable of discriminating between natively folded  $h\beta_2m$  and  $\Delta N6$  at pH 6.2 (Figure 1A).  $h\beta_2m$  was biotinylated (predominantly at the N-terminus and on Lys7 and/or Lys92) and immobilized as a target on streptavidin-coated magnetic beads, as described previously (30). The initial SELEX protocol used an N30 2'F-pyrimidine substituted RNA library, in order to create aptamers resistant to nucleases (25, 32), and included counter-selection against  $\Delta N6$  monomers immobilized as for  $h\beta_2m$ , as well as long-straight and worm-like amyloid fibrils formed from  $h\beta_2m$  at acidic pH (40). This protocol resulted in the removal of most

of the aptamers from the selected pool, consistent with the different protein conformers having many epitopes in common. We therefore abandoned counter-selections, except against biotin linker-blocked streptavidin beads alone. In addition, in the final round of SELEX, aptamers bound to bead-immobilized h $\beta_2$ m were competed off the beads using non-biotinylated h $\beta_2$ m in solution, in order to ensure that the selected aptamer pool contained ligands for native epitopes, SELEX was carried out at pH 6.2 as this is both optimal for h $\beta_2$ m/ $\Delta$ N6 co-polymerization (h $\beta_2$ m does not self-assemble spontaneously on a relevant timescale at this pH, whilst  $\Delta$ N6 assembles rapidly) (4) and is physiologically relevant for amyloid deposition in patients with DRA (41, 42). In total, 12 SELEX rounds were performed, with rounds 6-12 having increased stringency (Experimental Procedures). From the final pool 11 RNA clones were sequenced and aligned using the program AliBee (43). These were then clustered using the phylogenetic software Clustal Omega (44) (Figure 2A).

#### *Isolation of 2'F B6 and characterization of the binding affinity to h $\beta_2$ m*

Two aptamers, B6 and B9, contained the most frequently occurring sequence motifs within the sequenced clones and showed some motif similarities (Figures 2A and 2B). In order to identify which aptamer to utilize for further studies an initial binding assay was employed using SPR. Biotinylated h $\beta_2$ m,  $\Delta$ N6 or the non-amyloidogenic murine  $\beta_2$ m (m $\beta_2$ m) (45) were immobilized on separate flowcells and aptamer binding monitored at pH 6.2. 2'F B6 binds to h $\beta_2$ m with an apparent affinity of ~500 nM (red trace in Figure 2C), but did not bind  $\Delta$ N6 (dark green trace) or m $\beta_2$ m (light green trace). In contrast, binding of 2'F B9 was so weak that a  $K_d$  could not be determined (data not shown). The secondary structure of B6, computed via Mfold to be a stable stem-loop ( $\Delta G^\circ \sim -16$  kcal/mol) (35) (Figure 3A), was confirmed using enzymatic solution structure probing (Figure 3B). This analysis suggests that the selected region consists of an extended base-paired stem-loop interrupted by several single-stranded bulges with a terminal loop consisting of a poly-U tetraloop (highlighted in red in Figures 2B and 3A). Note, both Mfold and enzymatic probing were of transcripts containing natural pyrimidines. B9 is predicted to

have several equivalently stable structures that are all identical in the selected region, which forms a structure very similar to that of B6 around one of the bulges (Figure 3C). B9 differs radically at the terminal loop, however, which is composed of six purine nucleotides. It appears that the loop is the motif that provides much of the binding energy for the interaction of B6 with h $\beta_2$ m. Further characterization was therefore restricted to B6 and its derivatives.

A truncated 44 nucleotide version of the 110 nucleotide full-length B6 was produced encompassing nucleotides 22 to 59 with 2'OH (termed 2'OH B6min) (Figure 3D) or 2'F pyrimidines (termed 2'F B6min) (Figure 3E), i.e. all of the selected region defining the stem-loop with some stabilizing additional base-pairs. We examined the solution binding of 2'F B6min to native h $\beta_2$ m and  $\Delta$ N6 using fluorescence spectroscopy. H $\beta_2$ m has two tryptophan residues: Trp60, which lies in the DE loop (Figure 1A) and is solvent exposed, and Trp95, which lies towards the C-terminus of the 100-residue protein and is buried. Tryptophan fluorescence of h $\beta_2$ m can be used to probe changes in conformation or chemical environment upon aptamer binding, with Trp95 reporting on alterations within the hydrophobic core (46), whilst Trp60 is sensitive to ligand binding (at least in proximity to this residue) at the protein surface. The fluorescence emission spectrum of monomeric h $\beta_2$ m (1  $\mu$ M) was monitored upon titration with 2'F B6min. The results showed a decrease in tryptophan emission intensity (with little change in  $\lambda_{\text{max}}$ ), consistent with binding of 2'F B6min to the protein surface adjacent to Trp60. Fitting the normalized intensity of Trp fluorescence versus the concentration of 2'F B6min added (Figure 4A) (Experimental Procedures) yielded a Hill slope of  $0.99 \pm 0.06$ , suggesting a specific one-site binding event, with an  $EC_{50}$  of  $223 \pm 10$  nM. Similar assays using 2'OH B6min showed no binding to h $\beta_2$ m (Figure 4B), indicating that the 2'F modifications to the pyrimidines are required for tight binding, consistent with the contribution of the polyU tetraloop to affinity. The fluorescence assay also showed no binding of 2'F B6min to  $\Delta$ N6 monomers (Figure 4C), consistent with the SPR data with full-length aptamers. These results indicate, therefore, that 2'F B6min is capable of discriminating between h $\beta_2$ m and  $\Delta$ N6. 2'-fluororibose is known to prefer different sugar pucker

conformations compared with unmodified residues (O4'-endo versus C3'-endo, respectively (47)). This could alter the conformation of the tetra-loop and hence its interaction with the protein.

*Determining the binding interface of B6min with natively folded h $\beta_2$ m using NMR*

To determine whether binding of 2'F B6 to h $\beta_2$ m induces conformational changes in the protein and to map the binding site in residue-specific detail, 2'F B6min was titrated into  $^{15}\text{N}$ ,  $^{13}\text{C}$  labeled h $\beta_2$ m at 0, 0.25, 0.5, 1.0 and 2.0 molar equivalents at pH 6.2 and  $^1\text{H}$ - $^{15}\text{N}$  HSQC spectra were recorded. The  $^1\text{H}$ - $^{15}\text{N}$  HSQC spectrum of the 2:1 mixture of 2'F B6min and h $\beta_2$ m is shown in Figures 5A and 5B. Addition of 2'F B6min results in the appearance of new peaks in the spectrum and the loss of resonances assigned to native apo-h $\beta_2$ m indicating that the complex is in slow exchange with the apo-protein, as expected for a high affinity complex. The chemical shift changes involve some, but not all, resonances, indicative of binding of the aptamer to a specific surface. The  $^1\text{H}$ - $^{15}\text{N}$  HSQC spectrum of the h $\beta_2$ m-2'F B6min complex was assigned using a combination of 2D and 3D NMR techniques (Experimental Procedures) (Figure 6A). The low sample concentration (60  $\mu\text{M}$ ) and relatively large size of the complex (25.6 kDa) made assignment challenging. Of the 88 main-chain resonances in the  $^1\text{H}$ - $^{15}\text{N}$  HSQC spectrum of h $\beta_2$ m, 55 were successfully assigned. The assigned spectrum of the 2'F B6min-h $\beta_2$ m complex was then used to map the binding site for 2'F B6min on the surface of the protein. Residues with the largest chemical shift differences upon aptamer binding are located on the face of h $\beta_2$ m that contains the A, B, E, and D  $\beta$ -strands (Figures 6B and 6C). A significant number of residues in this region could not be assigned unambiguously in the spectrum of the complex, suggesting that they experience large chemical shift differences upon aptamer binding, or are not detected due to exchange line broadening (Figures 6B and 6C). The titration was also performed using 2'OH B6min (Figures 5C and 5D). No changes in the chemical shifts of h $\beta_2$ m were observed, even at the 2:1 aptamer: h $\beta_2$ m molar ratio, confirming that the presence of 2'F modified pyrimidines is vital for high affinity binding. To investigate whether 2'F B6min is able to recognize  $\Delta\text{N6}$ , 2 molar equivalents of the aptamer were added to 60  $\mu\text{M}$   $^{15}\text{N}$ -labeled  $\Delta\text{N6}$  and binding again assessed by monitoring changes in chemical shifts (Figures 5E

and 5F). In this sample the large changes in chemical shifts observed previously in the h $\beta_2$ m-2'F B6min complex (Figures 5A and 5B) were not detected (e.g. compare residues Lys41 and Ala79 in Figures 5B and 5F). For some resonances, small changes in chemical shift were observed, however, in those cases the chemical shifts did not saturate, even in the presence of a 2-fold molar excess of 2'F B6 (e.g. residues Ser20 and Cys80 (Figure 5F)). The results thus confirm a significantly lower affinity of this aptamer for  $\Delta\text{N6}$ .

To obtain more detailed information about the position of the 2'F B6min binding site on the surface of h $\beta_2$ m the intensity of each resonance was determined in the presence of a 2-fold molar excess of aptamer and compared with the intensity of its apo counterpart. The results of this analysis are shown in Figure 7A. Resonances arising from residues in the A, B, E, D  $\beta$ -strands, the AB and DE loops, residues 3-6 in the N-terminal region and the C-terminal 6 residues (red in Figure 7A) lose >80% of their intensity in the spectrum of the complex. These residues form a contiguous surface on h $\beta_2$ m (Figure 7A) and include the N-terminal 6 residues of h $\beta_2$ m that are lacking in  $\Delta\text{N6}$  and confer increased affinity, consistent with these residues forming part of the interface between the RNA and the protein. Consistent with this, there is little or no change in intensity for residues that lie in the CC' loop, F and G  $\beta$ -strands on the opposite face of h $\beta_2$ m (grey in Figure 7A). By contrast with these results, addition of a 2-fold molar excess of 2'OH B6min to h $\beta_2$ m has no significant effect on the intensities of the resonances of native h $\beta_2$ m (Figure 7B), consistent with its lack of binding.

A similar analysis was performed to assess the possible interaction between 2'F B6min and  $\Delta\text{N6}$ . As expected based on the fluorescence titration results shown in Figure 4C, little change in intensity was observed for the vast majority of residues in this sample (compare Figures 7A and 7C), consistent with weak binding to  $\Delta\text{N6}$ . Furthermore, the residues that do show a difference in resonance intensity differ from those involved in the 2'F B6min-h $\beta_2$ m interface. For example, while resonances belonging to residues in the AB loop, the E strand and the C-terminal 6 residues of native h $\beta_2$ m diminish in intensity by >80% upon interaction with 2'F B6min, these resonances are largely unaffected (retaining > 60%



average intensity) when  $\Delta N6$  is incubated with the aptamer. Moreover, the residues in  $\Delta N6$  showing the largest decrease in intensity upon addition of 2'F B6min (red in Figure 7C) are spread throughout the structure of the protein, suggesting that binding of 2'F B6min to  $\Delta N6$  is less specific than the 2'F B6-h $\beta_2m$  interaction. These differences in binding presumably explain the insensitivity of tryptophan fluorescence observed upon addition of 2'F B6min to  $\Delta N6$ .

The 2'F B6min-h $\beta_2m$  interface defined by these experiments (Figures 8A-C) includes a large number of aromatic side-chains (Y10, F22, Y26, F56, Y63, Y66 and Y67, green in Figure 8C), as often found in protein:RNA complexes (48). The residues involved in the binding interface might also be expected to be positively charged, but there appears to be an equal balance of positively charged residues (R3, K6, H13, K19, K48, H51, K94 (blue in Figure 8C)) and negatively charged side-chains (E16, D38, E50, D53, D59, E69, D98 (pink in Figure 8C)). Analysis of the NMR data shows that residues 3-6 are clearly part of the binding site. This sequence is absent in  $\Delta N6$ , which binds very poorly, and contains two positive charges (R3 and K6), but no negative charges. This region is therefore a candidate for a favorable electrostatic interaction with the aptamer. Indeed, m $\beta_2m$  which does not bind this aptamer (Figure 2C), has a Gln substituted for Lys at residue 6 (the N-terminal sequence of m $\beta_2m$  is IQKTPQ), implying that Lys6 is a likely key recognition element for h $\beta_2m$ .

### *2'F B6min alters the co-assembly of $\Delta N6$ and h $\beta_2m$*

The NMR and fluorescence data presented above indicate that 2'F B6min binds tightly to h $\beta_2m$ , but only weakly and non-specifically to  $\Delta N6$ . At pH 6.2 h $\beta_2m$  does not self-assemble into amyloid fibrils *in vitro* over a timescale of several weeks at a concentration of 40  $\mu M$ , even using significant agitation (13, 49, 50). In contrast,  $\Delta N6$  rapidly and quantitatively forms fibrils under these conditions (19, 49). When the two proteins are incubated together at this pH they co-polymerize, forming hetero-polymeric fibrils with distinct structural properties compared with either of their homopolymeric counterparts (4). To determine whether 2'F B6min is able to affect the co-aggregation of h $\beta_2m$  and  $\Delta N6$  (due to preferential binding of the

aptamer to one of the fibrillating monomers), the two proteins were mixed (each at a concentration of 40  $\mu M$ ) in the presence or absence of a 2-fold molar excess of 2'F B6min (160 $\mu M$ ) at pH 6.2. Assembly was monitored by separating soluble and insoluble material by centrifugation and subsequent analysis of each fraction by SDS PAGE (Experimental Procedures) (Figure 9). In parallel, a sample of the assembly products were monitored using transmission EM (TEM) to confirm whether amyloid fibrils were produced. The results of these experiments showed that in the absence of 2'F B6min each protein remains in the soluble fraction up to the 24 h time point, after which time insoluble material containing both proteins forms (Figure 9A). After 166 h of incubation both proteins are also found in the pellet presumably due to their co-polymerization into fibrils (4). By contrast, in the presence of 2'F B6min aggregation occurs more rapidly, with >90 % of  $\Delta N6$  and ~ 40% of h $\beta_2m$  forming fibrillar material after 24 h. TEM images of the samples after 166 h confirmed that the insoluble material in the pellets contains amyloid fibrils (Figure 9A, B), although the precise location of each protein within each fibril (i.e. the extent to which co-polymerization occurred) could not be ascertained from these experiments. Presumably, the interaction between soluble  $\Delta N6$  and h $\beta_2m$  is inhibited by 2'F B6min, leading to rapid polymerization of  $\Delta N6$  which in part co-polymerizes with h $\beta_2m$ .

## DISCUSSION

In order to derive a structural mechanism of amyloid formation the identity and structure of all assembling components must be defined and how these species interact and form the cross- $\beta$  structure of amyloid determined. Here, RNA SELEX has been used to generate a specific, high-affinity aptamer (2'F B6) against monomeric h $\beta_2m$ . Importantly, despite only subtle differences in the structures of monomeric h $\beta_2m$  and its N-terminal truncation variant  $\Delta N6$  at pH 6.2 (Figure 1A, B), 2'F B6 is able to discriminate between these structures, showing tight and highly specific binding to the  $\beta$ -sheet containing the A, B, E, D strands of h $\beta_2m$ . By contrast, weak, non-specific binding is observed to  $\Delta N6$  that is detectable only at the high protein and RNA concentrations used for NMR (60  $\mu M$  protein). The discrimination between h $\beta_2m$  and  $\Delta N6$  by 2'F B6 can be

explained, at least in part, by the presence of Lys6 in the binding interface. However, given that the binding interface appears to involve an extended region spanning the A, B, E and D  $\beta$ -strands, other residues must also contribute to affinity. Indeed, differences in the organization of residues on the surfaces of h $\beta_2$ m and  $\Delta$ N6 that result from the isomerization of the X-Pro32 peptide bond from the native *cis* isomer in h $\beta_2$ m to the *trans* isomer in  $\Delta$ N6 (19), and/or the decreased stability (13) and increased conformational dynamics of  $\Delta$ N6 compared with h $\beta_2$ m (19), may also contribute to 2'F B6 discriminating between these otherwise similar structures. For example, although the structure of the backbone is highly conserved between h $\beta_2$ m and  $\Delta$ N6 (Figure 1B), the orientation of the side-chains of aromatic residues involved in the aptamer binding interface differs significantly (Figure 10A). Furthermore, the organization of hydrophobic and charged residues on the surface formed by the A, B, E, D  $\beta$ -strands in h $\beta_2$ m differs significantly from  $\Delta$ N6 (Figure 10B). Accordingly, the apical region of this surface in h $\beta_2$ m is more highly positively charged than its equivalent in  $\Delta$ N6 (this region contains the N-terminal six amino acids, including Lys6) (Figure 10B). In addition, the organization of negatively charged residues (involving the AB loop, the EF loop and the C-terminus) also differs between the two proteins (Figure 10B). In total, therefore, the balance between electrostatic and hydrophobic residues, crucial for nucleic acid binding (51), is distinct in h $\beta_2$ m and  $\Delta$ N6, partly due to the removal of the N-terminal six amino acids, and partly due to differences in solvent exposure of hydrophobic residues in the DE and BC loops in the two proteins that occur as a consequence of X-Pro32 isomerization.

The role of  $\Delta$ N6 in DRA is not currently understood. Whilst  $\Delta$ N6 is present in the amyloid deposits found in patients with DRA (52), it remains unknown whether the N-terminal truncation of h $\beta_2$ m occurs pre- or post- fibril formation. Additionally, the interaction between h $\beta_2$ m and  $\Delta$ N6 *in vitro* is complex, with  $\Delta$ N6 possessing the ability to convert monomeric h $\beta_2$ m into an amyloidogenic conformation (4, 19, 53) and to act as a fibrillar seed able to be elongated with h $\beta_2$ m monomers (19, 49). The aptamer selected here may be useful as an analytical probe to derive greater clarity in understanding the early stages of h $\beta_2$ m and  $\Delta$ N6 co-assembly into

amyloid. Given the complexity of amyloid formation, where self-assembly can be initiated by one or more rare conformers that may differ subtly in structure, and that different oligomeric species may exhibit profoundly different cytotoxicity (54, 55), RNA aptamers offer unique potentials as reagents for the analysis of, and interference with, amyloid formation.

The specific and tight binding of 2'F B6 to h $\beta_2$ m alters the course of amyloid assembly in mixtures of h $\beta_2$ m and  $\Delta$ N6 at pH 6.2. Thus, aptamer binding to h $\beta_2$ m disfavors the incorporation of h $\beta_2$ m into amyloid fibrils during co-assembly with  $\Delta$ N6 and results in more rapid fibril formation. In the presence of the aptamer h $\beta_2$ m molecules will become incorporated into fibrils only after aptamer dissociation, possibly by cross-seeding with preformed  $\Delta$ N6 fibrils (4, 49). Alternatively,  $\Delta$ N6 may promote conversion of h $\beta_2$ m to an amyloidogenic conformation once 2'F B6min dissociates (4, 19, 53), pulling the equilibrium towards co-assembly into fibrils. Given that amyloid formation is under kinetic control, the development of aptamers able to bind their targets with slow off-rates (even for the same apparent  $K_d$ ) would provide an effective strategy to control assembly. Such aptamers could be isolated by increasing the length of time of the elution steps in SELEX as stringency is increased. Alternatively, coupling of the RNA aptamer to molecule with known affinity to the target could provide a route to achieving this goal by exploiting avidity effects. Doxycycline, a small molecule tetracycline analogue, has been shown to modulate the formation of h $\beta_2$ m fibrils *in vitro* (56), to reduce articular pain and improve movement in DRA patients (57) and to correct a locomotory defect in *C.elegans* expressing h $\beta_2$ m (58). Analysis of the h $\beta_2$ m-doxycycline complex using NMR suggests that the highest affinity binding site ( $IC_{50} \sim 50 \mu M$  (56)) involves residues that lie in the C-terminal region of strand A, the N-terminal region of strand B and the central residues of the AB loop (56). A second, lower affinity, binding site involves the N-terminal region and residues in the BC and DE loops. An intriguing possibility, therefore, would be to create an aptamer linked to doxycycline such that the relatively tight and specific binding of 2'F B6 can be exploited to enhance binding of doxycycline to its target interface. Creation of such bipartite molecules have been shown to be a highly effective strategy, not just for enhancing the

effectiveness of RNA aptamers as delivery vehicles (59-61), but in many other applications (62-64).

In conclusion, the biophysical and biochemical studies presented here demonstrate that RNA aptamers can be highly specific and discriminatory probes, modulating co-polymerization reactions and controlling the course of amyloid assembly. How the 2'F B6-h $\beta_2$ m complex changes as fibril formation proceeds and the effect of the aptamer on hetero-polymorphic fibril structure and stability will require further studies, for example, by exploiting the powers of solid-state NMR to analyze fibril structures (65, 66). Further characterization and modification of 2'F B6 will potentially allow the affinity of the aptamer for h $\beta_2$ m to be increased, and selection of aptamers specific for  $\Delta$ N6 will also allow detailed biophysical analysis of the role of  $\Delta$ N6 in h $\beta_2$ m-

$\Delta$ N6 co-polymerization. Understanding this process further may shed light on the molecular mechanisms of fibril formation and how the protein precursors of hetero-polymeric assemblies can be modulated to tailor the extent, rate, and structure of amyloid fibrils.

#### ACKNOWLEDGEMENTS

We thank members of our research groups for helpful discussion and comments. We acknowledge with thanks the Medical Research Council (grant 0900958) for funding CJS, SJW, DHJB and AMB, the Wellcome Trust (089311/z/09/z) and the European Research Council under the European Union's Seventh Framework Programme (*FP7/2007-2013*) (ERC grant number 322408) for funding TKK. We also acknowledge the Wellcome Trust for funding the NMR facility (094232).

## REFERENCES

1. Eisenberg, D., and Jucker, M. (2012) The amyloid state of proteins in human diseases. *Cell* **148**, 1188–1203
2. Berthelot, K., Cullin, C., and Lecomte, S. (2013) What does make an amyloid toxic: Morphology, structure or interaction with membrane? *Biochimie* **95**, 12–19
3. Chiti, F., and Dobson, C. M. (2009) Amyloid formation by globular proteins under native conditions. *Nat. Chem. Biol.* **5**, 15–22
4. Sarell, C. J., Woods, L. A., Su, Y., Debelouchina, G. T., Ashcroft, A. E., Griffin, R. G., Stockley, P. G., and Radford, S. E. (2013) Expanding the repertoire of amyloid polymorphs by copolymerization of related protein precursors. *J. Biol. Chem.* **288**, 7327–7337
5. Lee, C. F., Bird, S., Shaw, M., Jean, L., and Vaux, D. J. (2012) Combined effects of agitation, macromolecular crowding, and interfaces on amyloidogenesis. *J. Biol. Chem.* **287**, 38006–38019
6. O'Nuallain, B., Williams, A. D., Westermarck, P., and Wetzel, R. (2004) Seeding specificity in amyloid growth induced by heterologous fibrils. *J. Biol. Chem.* **279**, 17490–17499
7. Pauwels, K., Williams, T. L., Morris, K. L., Jonckheere, W., Vandersteen, A., Kelly, G., Schymkowitz, J., Rousseau, F., Pastore, A., Serpell, L. C., and Broersen, K. (2012) Structural basis for increased toxicity of pathological A $\beta$  42:A $\beta$  40 ratios in Alzheimer's disease. *J. Biol. Chem.* **287**, 5650–5660
8. Seeliger, J., Evers, F., Jeworrek, C., Kapoor, S., Weise, K., Andreetto, E., Tolan, M., Kapurniotu, A., and Winter, R. (2012) Cross-amyloid interaction of A $\beta$  and IAPP at lipid membranes. *Angew. Chem. Int. Ed.* **51**, 679–683
9. Giasson, B. I., Forman, M. S., Higuchi, M., Golbe, L. I., Graves, C. L., Kotzbauer, P. T., Trojanowski, J. Q., and Lee, V. M. (2003) Initiation and synergistic fibrillization of tau and  $\alpha$ -synuclein. *Science* **300**, 636–640
10. MacPhee, C. E., and Dobson, C. M. (2000) Formation of mixed fibrils demonstrates the generic nature and potential utility of amyloid nanostructures. *J. Am. Chem. Soc.* **122**, 12707–12713
11. Neudecker, P., Robustelli, P., Cavalli, A., Walsh, P., Lundstrom, P., Zarrine-Afsar, A., Sharpe, S., Vendruscolo, M., and Kay, L. E. (2012) Structure of an intermediate state in protein folding and aggregation. *Science* **336**, 362–366
12. Lu, J.-X., Qiang, W., Yau, W.-M., Schwieters, C. D., Meredith, S. C., and Tycko, R. (2013) Molecular structure of  $\beta$ -amyloid fibrils in Alzheimer's disease brain tissue. *Cell* **154**, 1257–1268
13. Eichner, T., and Radford, S. E. (2009) A generic mechanism of  $\beta_2$ -microglobulin amyloid assembly at neutral pH involving a specific proline switch. *J. Mol. Biol.* **386**, 1312–1326
14. Platt, G. W., and Radford, S. E. (2009) Glimpses of the molecular mechanisms of beta2-microglobulin fibril formation in vitro: aggregation on a complex energy landscape. *FEBS lett.* **583**, 2623–2629
15. Kad, N. M., Thomson, N. H., Smith, D. P., Smith, D. A., and Radford, S. E. (2001) B $_2$ -microglobulin and its deamidated variant, N17D form amyloid fibrils with a range of morphologies in vitro. *J. Mol. Biol.* **313**, 559–571
16. Yamamoto, S., Hasegawa, K., Yamaguchi, I., Tsutsumi, S., Kardos, J., Goto, Y., Gejyo, F., and Naiki, H. (2004) Low concentrations of sodium dodecyl sulfate induce the extension of  $\beta_2$ -microglobulin-related amyloid fibrils at a neutral pH. *Biochemistry* **43**, 11075–11082
17. Hodkinson, J. P., Radford, S. E., and Ashcroft, A. E. (2012) The role of conformational flexibility in  $\beta_2$ -microglobulin amyloid fibril formation at neutral pH. *Rapid Commun. Mass Spectrom.* **26**, 1783–1792
18. Eakin, C. M., Berman, A. J., and Miranker, A. D. (2006) A native to amyloidogenic transition regulated by a backbone trigger. *Nat. Struct. Mol. Biol.* **13**, 202–208
19. Eichner, T., Kalverda, A. P., Thompson, G. S., Homans, S. W., and Radford, S. E. (2011) Conformational conversion during amyloid formation at atomic resolution. *Mol. Cell* **41**, 161–172
20. Esposito, G., Michelutti, R., Verdone, G., Viglino, P., Hernandez, H., Robinson, C. V., Amoresano, A., Dal Piaz, F., Monti, M., Pucci, P., Mangione, P., Stoppini, M., Merlini, G., Ferri, G., and Bellotti, V. (2000) Removal of the N-terminal hexapeptide from human  $\beta_2$ -microglobulin



- facilitates protein aggregation and fibril formation. *Protein Sci.* **9**, 831–845
21. Sakata, M., Chatani, E., Kameda, A., Sakurai, K., Naiki, H., and Goto, Y. (2008) Kinetic coupling of folding and prolyl isomerization of  $\beta_2$ -microglobulin studied by mutational analysis. *J. Mol. Biol.* **382**, 1242–1255
  22. Jahn, T. R., Parker, M. J., Homans, S. W., and Radford, S. E. (2006) Amyloid formation under physiological conditions proceeds via a native-like folding intermediate. *Nat. Struct. Mol. Biol.* **13**, 195–201
  23. Rhie, A., Kirby, L., Sayer, N., Wellesley, R., Disterer, P., Sylvester, I., Gill, A., Hope, J., James, W., and Tahiri-Alaoui, A. (2003) Characterization of 2'-fluoro-RNA aptamers that bind preferentially to disease-associated conformations of prion protein and inhibit conversion. *J. Biol. Chem.* **278**, 39697–39705
  24. Mashima, T., Nishikawa, F., Kamatari, Y. O., Fujiwara, H., Saimura, M., Nagata, T., Kodaki, T., Nishikawa, S., Kuwata, K., and Katahira, M. (2013) Anti-prion activity of an RNA aptamer and its structural basis. *Nucleic Acids Res.* **41**, 1355–1362
  25. Ylera, F., Lurz, R., Erdmann, V. A., and Fürste, J. P. (2002) Selection of RNA aptamers to the Alzheimer's disease amyloid peptide. *Biochem. Biophys. Res. Comm.* **290**, 1583–1588
  26. Takahashi, T., Tada, K., and Mihara, H. (2009) RNA aptamers selected against amyloid  $\beta$ -peptide (A $\beta$ ) inhibit the aggregation of A $\beta$ . *Mol. Biosyst.* **5**, 986
  27. Farrar, C. T., William, C. M., Hudry, E., Hashimoto, T., and Hyman, B. T. (2014) RNA aptamer probes as optical imaging agents for the detection of amyloid plaques. *PLoS ONE* **9**, e89901
  28. Tsukakoshi, K., Abe, K., Sode, K., and Ikebukuro, K. (2012) Selection of DNA aptamers that recognize  $\alpha$ -synuclein oligomers using a competitive screening method. *Anal. Chem.* **84**, 5542–5547
  29. Rahimi, F., Murakami, K., Summers, J. L., Chen, C.-H. B., and Bitan, G. (2009) RNA aptamers generated against oligomeric A $\beta$ 40 recognize common amyloid aptatopes with low specificity but high sensitivity. *PLoS ONE* **4**, e7694
  30. Bunka, D. H. J., Mantle, B. J., Morten, I. J., Tennent, G. A., Radford, S. E., and Stockley, P. G. (2007) Production and characterization of RNA aptamers specific for amyloid fibril epitopes. *J. Biol. Chem.* **282**, 34500–34509
  31. Debelouchina, G. T., Platt, G. W., Bayro, M. J., Radford, S. E., and Griffin, R. G. (2010) Intermolecular alignment in  $\beta_2$ -microglobulin amyloid fibrils. *J. Am. Chem. Soc.* **132**, 17077–17079
  32. Padilla, R., and Sousa, R. (2002) A Y639F/H784A T7 RNA polymerase double mutant displays superior properties for synthesizing RNAs with non-canonical NTPs. *Nucleic Acids Res.* **30**, e138
  33. Adams, C. J., Murray, J. B., Arnold, J. R. P., and Stockley, P. G. (1994) A convenient synthesis of S-cyanoethyl-protected 4-thiouridine and its incorporation into oligoribonucleotides. *Tetrahedron Lett* **35**, 765–768
  34. Murray, J. B., Collier, A. K., and Arnold, J. R. (1994) A general purification procedure for chemically synthesized oligoribonucleotides. *Anal. Biochem.* **218**, 177–184
  35. Zuker, M. (2003) Mfold web server for nucleic acid folding and hybridization prediction. *Nucleic Acids Res.* **31**, 3406–3415
  36. Lakowicz, J. R. (1999) *Principles of Fluorescence Spectroscopy*, 2<sup>nd</sup> Ed., Springer
  37. Kupče, Ě., Nishida, T., and Freeman, R. (2003) Hadamard NMR spectroscopy. *Prog. Nucl. Magn. Reson. Spectr.* **42**, 95–122
  38. Vranken, W. F., Boucher, W., Stevens, T. J., Fogh, R. H., Pajon, A., Llinas, M., Ulrich, E. L., Markley, J. L., Ionides, J., and Laue, E. D. (2005) The CCPN data model for NMR spectroscopy: development of a software pipeline. *Proteins* **59**, 687–696
  39. Xue, W. F., Homans, S. W., and Radford, S. E. (2008) Systematic analysis of nucleation-dependent polymerization reveals new insights into the mechanism of amyloid self-assembly. *Proc. Natl. Acad. Sci. USA* **105**, 8926–8931
  40. Gosal, W. S., Morten, I. J., Hewitt, E. W., Smith, D. A., Thomson, N. H., and Radford, S. E. (2005) Competing pathways determine fibril morphology in the self-assembly of  $\beta_2$ -microglobulin into amyloid. *J. Mol. Biol.* **351**, 850–864

41. Ward, T. T., and Steigbigel, R. T. (1978) Acidosis of synovial fluid correlates with synovial fluid leukocytosis. *Am. J. Med.* **64**, 933–936
42. Relini, A., Canale, C., De Stefano, S., Rolandi, R., Giorgetti, S., Stoppini, M., Rossi, A., Fogolari, F., Corazza, A., Esposito, G., Gliozzi, A., and Bellotti, V. (2006) Collagen plays an active role in the aggregation of  $\beta_2$ -microglobulin under physiopathological conditions of dialysis-related amyloidosis. *J. Biol. Chem.* **281**, 16521–16529
43. Leontovich, A. M., Brodsky, L. I., Drachev, V. A., and Nikolaev, V. K. (2002) Adaptive algorithm of automated annotation. *Bioinformatics* **18**, 838–846
44. Sievers, F., Wilm, A., Dineen, D., Gibson, T. J., Karplus, K., Li, W. Z., Lopez, R., McWilliam, H., Remmert, M., Soding, J., Thompson, J. D., and Higgins, D. G. (2011) Fast, scalable generation of high-quality protein multiple sequence alignments using Clustal Omega. *Mol. Syst. Biol.* **7**
45. Ivanova, M. I. (2004) An amyloid-forming segment of  $\beta_2$ -microglobulin suggests a molecular model for the fibril. *Proc. Natl. Acad. Sci. USA* **101**, 10584–10589
46. Chatani, E., Ohnishi, R., Konuma, T., Sakurai, K., Naiki, H., and Goto, Y. (2010) Pre-steady-state kinetic analysis of the elongation of amyloid fibrils of  $\beta_2$ -microglobulin with tryptophan mutagenesis. *J. Mol. Biol.* **400**, 1057–1066
47. Berger, I., Tereshko, V., Ikeda, H., Marquez, V. E., and Egli, M. (1998) Crystal structures of B-DNA with incorporated 2'-deoxy-2'-fluoro-arabino-furanosyl thymines: implications of conformational preorganization for duplex stability. *Nucleic Acids Res.* **26**, 2473–2480
48. Baker, C. M., and Grant, G. H. (2007) Role of aromatic amino acids in protein-nucleic acid recognition. *Biopolymers* **85**, 456–470
49. Mangione, P. P., Esposito, G., Relini, A., Raimondi, S., Porcari, R., Giorgetti, S., Corazza, A., Fogolari, F., Penco, A., Goto, Y., Lee, Y. H., Yagi, H., Cecconi, C., Naqvi, M. M., Gillmore, J. D., Hawkins, P. N., Chiti, F., Rolandi, R., Taylor, G. W., Pepys, M. B., Stoppini, M., and Bellotti, V. (2013) Structure, folding dynamics and amyloidogenesis of Asp76Asn  $\beta_2$ -microglobulin: roles of shear flow, hydrophobic surfaces and alpha crystallin. *J. Biol. Chem.* **288**, 30917–30930
50. Myers, S. L., Jones, S., Jahn, T. R., Morten, I. J., Tennent, G. A., Hewitt, E. W., and Radford, S. E. (2006) A systematic study of the effect of physiological factors on  $\beta_2$ -microglobulin amyloid formation at neutral pH. *Biochemistry* **45**, 2311–2321
51. Marcovitz, A., and Levy, Y. (2011) Frustration in protein–DNA binding influences conformational switching and target search kinetics. *Proc. Natl. Acad. Sci. USA* **108**, 17957–17962
52. Bellotti, V., Stoppini, M., Mangione, P., Sunde, M., Robinson, C., Asti, L., Brancaccio, D., and Ferri, G. (1998) Beta2-microglobulin can be refolded into a native state from ex vivo amyloid fibrils. *Eur. J. Biochem.* **258**, 61–67
53. Karamanos, T. K., Kalverda, A. P., Thompson, G. S., and Radford, S. E. (2014) Visualization of transient protein-protein interactions that promote or inhibit amyloid assembly. *Mol. Cell*, in press
54. Cremades, N., Cohen, S. I. A., Deas, E., Abramov, A. Y., Chen, A. Y., Orte, A., Sandal, M., Clarke, R. W., Dunne, P., Aprile, F. A., Bertocini, C. W., Wood, N. W., Knowles, T. P. J., Dobson, C. M., and Klenerman, D. (2014) Direct observation of the interconversion of normal and toxic forms of  $\alpha$ -synuclein. *Cell* **149**, 1048–1059
55. Campioni, S., Mannini, B., Zampagni, M., Pensalfini, A., Parrini, C., Evangelisti, E., Relini, A., Stefani, M., Dobson, C. M., Cecchi, C., and Chiti, F. (2010) A causative link between the structure of aberrant protein oligomers and their toxicity. *Nat. Chem. Biol.* **6**, 140–147
56. Giorgetti, S., Raimondi, S., Pagano, K., Relini, A., Bucciattini, M., Corazza, A., Fogolari, F., Codutti, L., Salmona, M., Mangione, P., Colombo, L., De Luigi, A., Porcari, R., Gliozzi, A., Stefani, M., Esposito, G., Bellotti, V., and Stoppini, M. (2011) Effect of tetracyclines on the dynamics of formation and deconstruction of  $\beta_2$ -microglobulin amyloid fibrils. *J. Biol. Chem.* **286**, 2121–2131
57. Montagna, G., Cazzulani, B., Obici, L., Uggetti, C., Giorgetti, S., Porcari, R., Ruggiero, R., Mangione, P. P., Brambilla, M., Lucchetti, J., Guiso, G., Gobbi, M., Merlini, G., Salmona, M., Stoppini, M., Villa, G., and Bellotti, V. (2013) Benefit of doxycycline treatment on articular disability caused by dialysis related amyloidosis. *Amyloid* **20**, 173–178

58. Diomede, L., Soria, C., Romeo, M., Giorgetti, S., Marchese, L., Mangione, P. P., Porcari, R., Zorzoli, I., Salmona, M., Bellotti, V., and Stoppini, M. (2012) *C. elegans* expressing human  $\beta_2$ -microglobulin: a novel model for studying the relationship between the molecular assembly and the toxic phenotype. *PLoS ONE* **7**, e52314
59. Chen, C.-H. B., Dellamaggiore, K. R., Ouellette, C. P., Sedano, C. D., Lizadjohry, M., Chernis, G. A., Gonzales, M., Baltasar, F. E., Fan, A. L., Myerowitz, R., and Neufeld, E. F. (2008) Aptamer-based endocytosis of a lysosomal enzyme. *Proc. Natl. Acad. Sci. USA* **105**, 15908–15913
60. McNamara, J. O., Andrechek, E. R., Wang, Y., Viles, K. D., Rempel, R. E., Gilboa, E., Sullenger, B. A., and Giangrande, P. H. (2006) Cell type-specific delivery of siRNAs with aptamer-siRNA chimeras. *Nat. Biotechnol.* **24**, 1005–1015
61. Zhou, J., Swiderski, P., Li, H., Zhang, J., Neff, C. P., Akkina, R., and Rossi, J. J. (2009) Selection, characterization and application of new RNA HIV gp 120 aptamers for facile delivery of Dicer substrate siRNAs into HIV infected cells. *Nucleic Acids Res.* **37**, 3094–3109
62. Rockey, W. M., Huang, L., Kloepping, K. C., Baumhover, N. J., Giangrande, P. H., and Schultz, M. K. (2011) Synthesis and radiolabeling of chelator-RNA aptamer bioconjugates with copper-64 for targeted molecular imaging. *Bioorg. Med. Chem.* **19**, 4080–4090
63. Huang, Y. Z., Hernandez, F. J., Gu, B., Stockdale, K. R., Nanapaneni, K., Scheetz, T. E., Behlke, M. A., Peek, A. S., Bair, T., Giangrande, P. H., and McNamara, J. O. (2012) RNA aptamer-based functional ligands of the neurotrophin receptor, TrkB. *Mol. Pharmacol.* **82**, 623–635
64. Bunka, D. H. J., Platonova, O., and Stockley, P. G. (2010) Development of aptamer therapeutics. *Curr. Opin. Pharmacol.* **10**, 557–562
65. Debelouchina, G. T., Platt, G. W., Bayro, M. J., Radford, S. E., and Griffin, R. G. (2010) Magic angle spinning NMR analysis of  $\beta_2$ -microglobulin amyloid fibrils in two distinct morphologies. *J. Am. Chem. Soc.* **132**, 10414–10423
66. Su, Y., Sarell, C. J., Eddy, M. T., Debelouchina, G. T., Andreas, L. B., Pashley, C. L., Radford, S. E., and Griffin, R. G. (2014) Secondary structure in the core of amyloid fibrils formed from human  $\beta_2$ m and its truncated variant  $\Delta$ N6. *J. Am. Chem. Soc.* **136**, 6313–6325

## FIGURES AND FIGURE LEGENDS

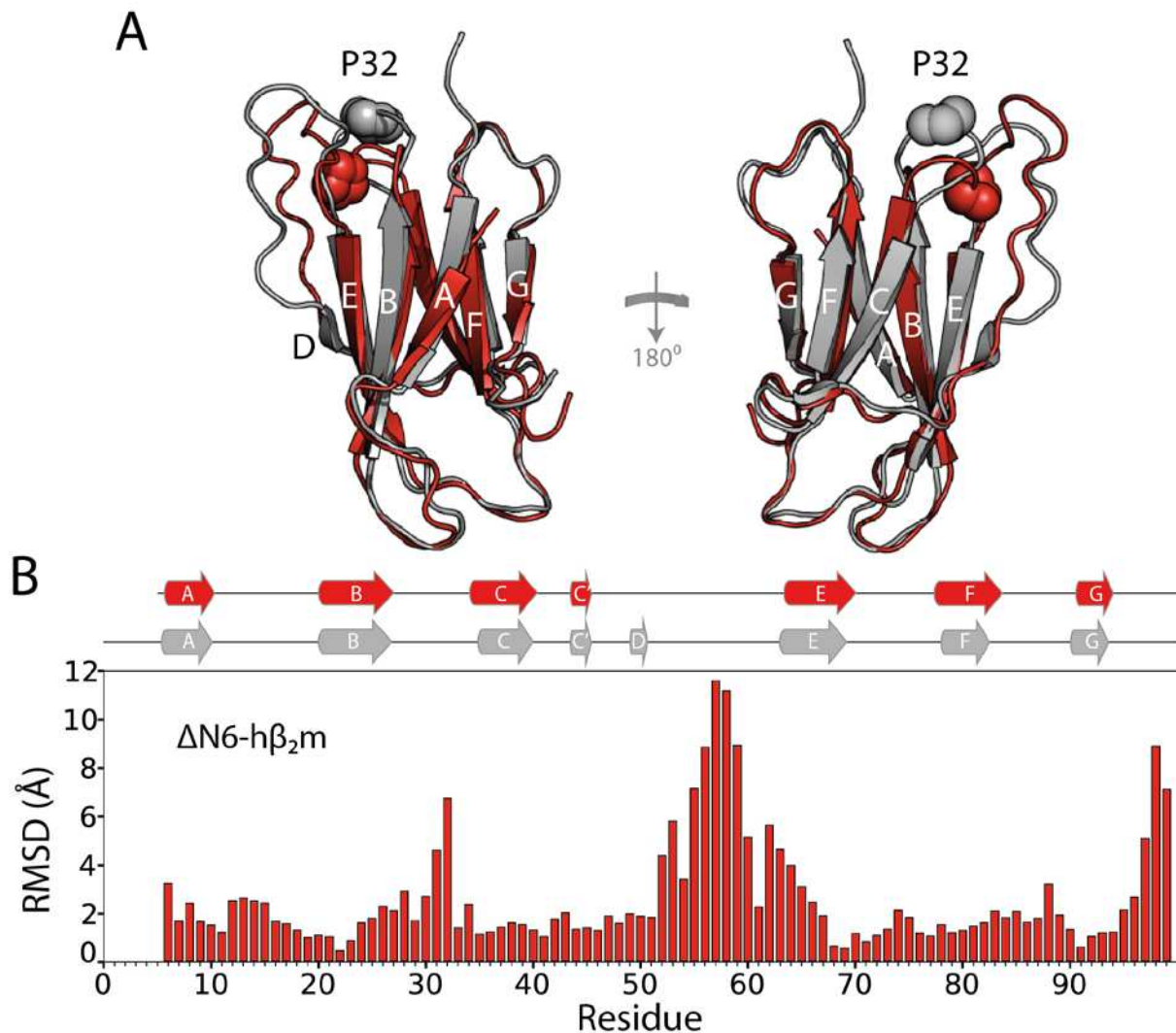


**Figure 1. Comparison of the structures of hβ<sub>2</sub>m and ΔN6.** (A) The structure of hβ<sub>2</sub>m (grey ribbon, PDB code: 2XKS (19)) and ΔN6 (red cartoon, PDB code: 2XKU (19)). The two β-sheets of the proteins comprising the A, B, E and D β-strands and the C, F and G β-strands are shown. Pro32 is shown in space fill. (B) Per-residue RMSD chart for the backbone atoms of hβ<sub>2</sub>m and ΔN6 (overall backbone RMSD ~1.5Å). The positions of the β-strands in these proteins are shown on top as grey (hβ<sub>2</sub>m) and red (ΔN6) ribbons.



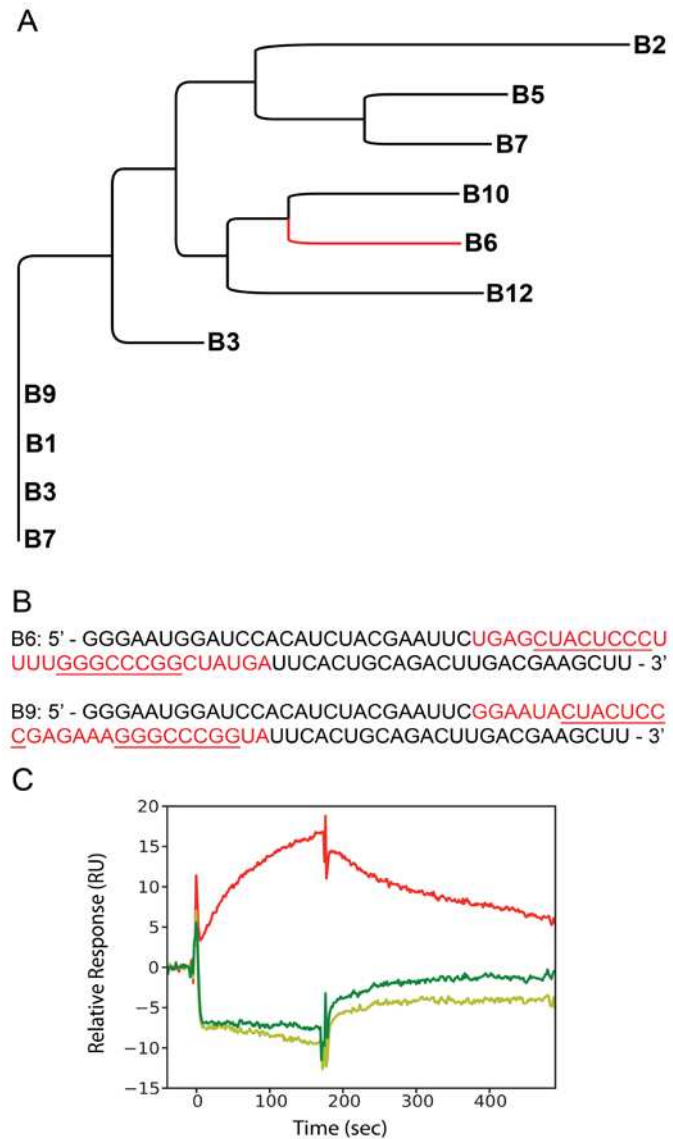


**Figure 2. Aptamer selection.** (A) The relationship of B6 to the 10 other sequences from the SELEX pool. (B) Sequences of aptamers B6 and B9. The selected regions are shown in red and their common sequence motifs are underlined. (C) SPR traces generated upon incubation of 1  $\mu$ M 2'F B6 (50 mM MES buffer, 120 mM NaCl, pH 6.2) over flow-cells immobilized with h $\beta_2$ m (red),  $\Delta$ N6 (dark green) or murine  $\beta_2$ m (light green).

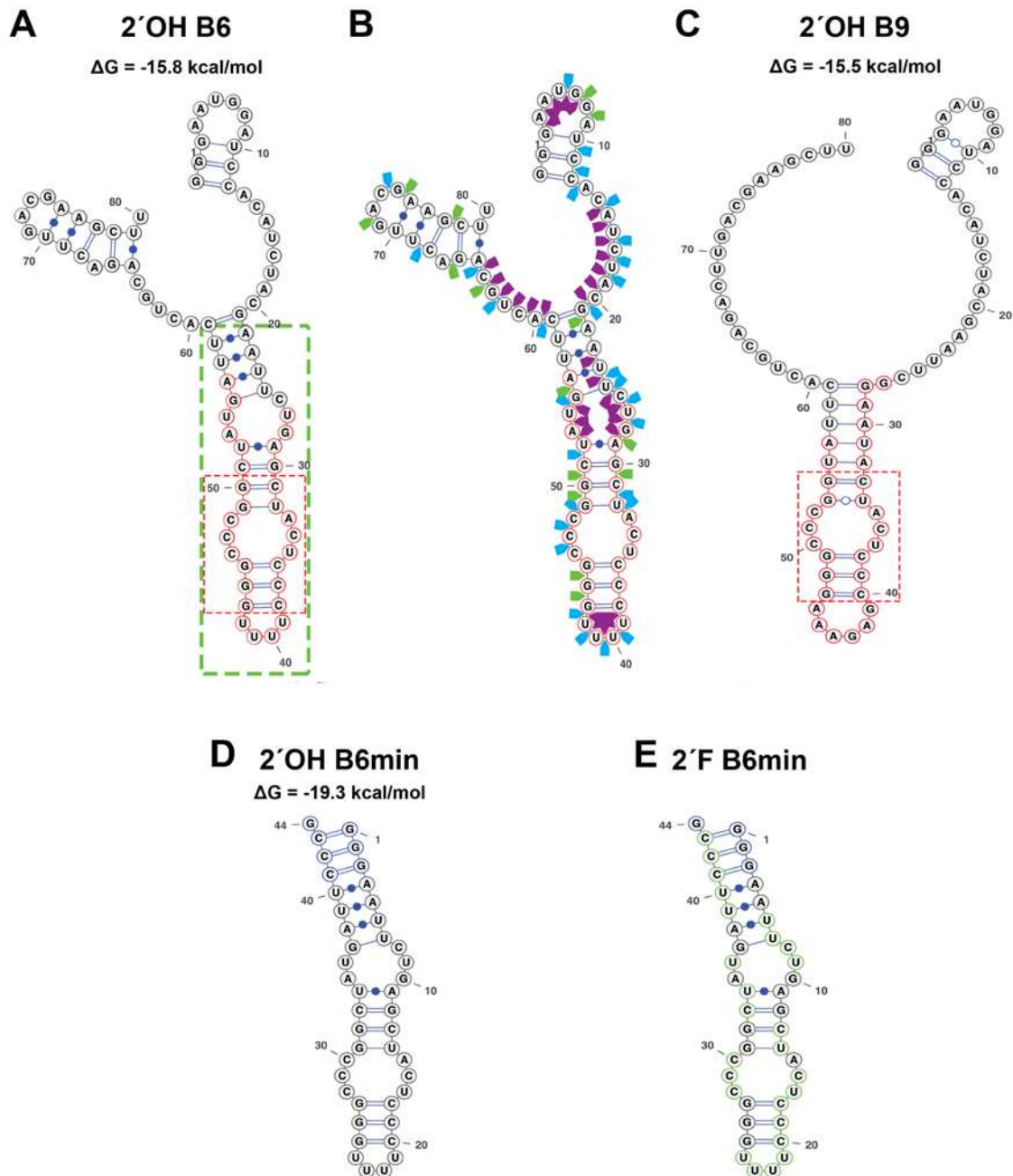


**Figure 3. Secondary structures of the B6 and B9 aptamers.** (A) The Mfold secondary structure prediction of the full length B6 aptamer with the nucleotides within the green box showing the region truncated to create the B6min aptamer sequence. Nucleotides circled in red define the random region. (B) Enzymatic solution structure probing of the full length B6 transcript with the random region highlighted in red. Cleavage sites by the G-specific RNase T1 (green arrows), U and C-specific RNase A (blue arrows) and single-stranded RNA specific S1 nuclease (purple arrows) are shown. (C) The Mfold of the full length B9 aptamer with the selected region highlighted as in (A). The dotted red boxes in (A) and (C) showed the conserved sequences and secondary structure elements of both aptamers.. (D) Secondary structure of 2'OH B6min and (E) 2'F B6min stem-loops. These have additional 5'-GGG and 3'-CCCG sequences added to increase their folded stability. 2'F pyrimidines are circled in green in (E).

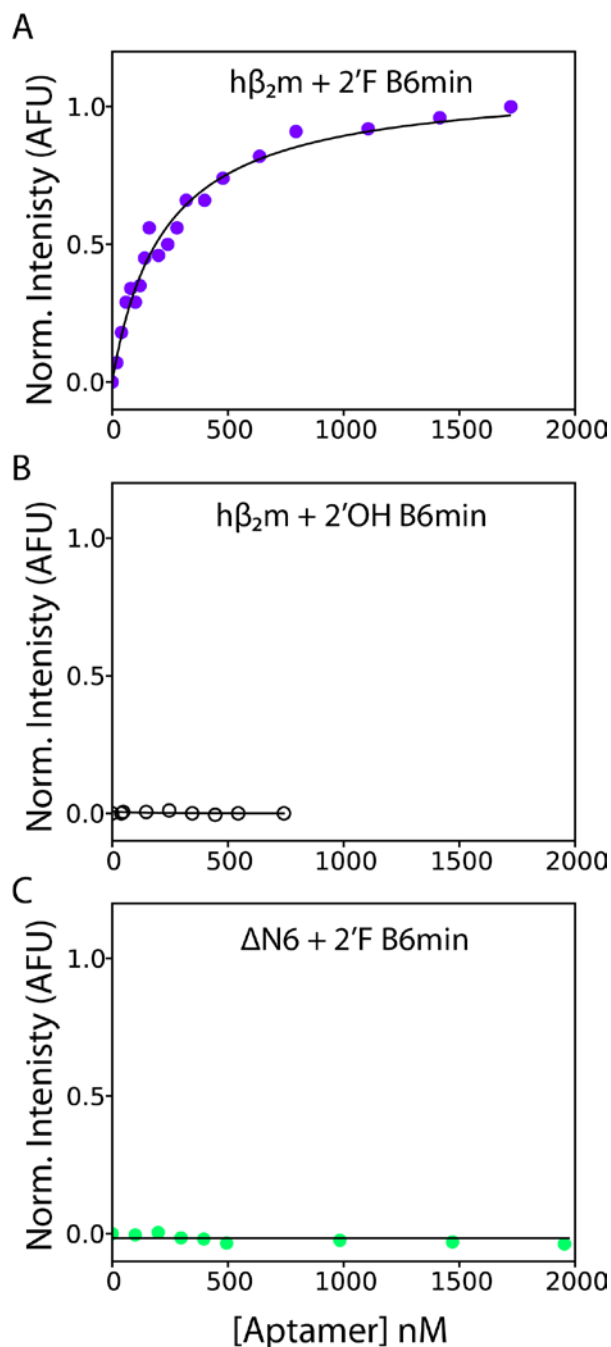


**Figure 4. Binding of 2'OH B6min and 2'F B6min to hβ<sub>2</sub>m and ΔN6 measured using intrinsic tryptophan fluorescence.** (A) Normalized tryptophan fluorescence of hβ<sub>2</sub>m (1 μM) upon addition of 2'F B6min (0 - 1.7 μM). The data are fitted to a logistic equation (solid line). The data are normalized between 0 (no aptamer) and 1 (the fluorescence signal in the presence of 1.7 μM aptamer) (Experimental Procedures). (B) Titration of hβ<sub>2</sub>m (1 μM) with 2'OH B6min. (C) Titration of ΔN6 (1 μM) with 2'F B6min. No fluorescence change was observed over the concentrations of aptamer added in (B) and (C). These data were normalized between 0 (no aptamer) and 1 (the fluorescence signal when 1.7 μM of 2'F B6min was added to hβ<sub>2</sub>m). All experiments were performed in 50 mM MES buffer, 120 mM NaCl, pH 6.2.

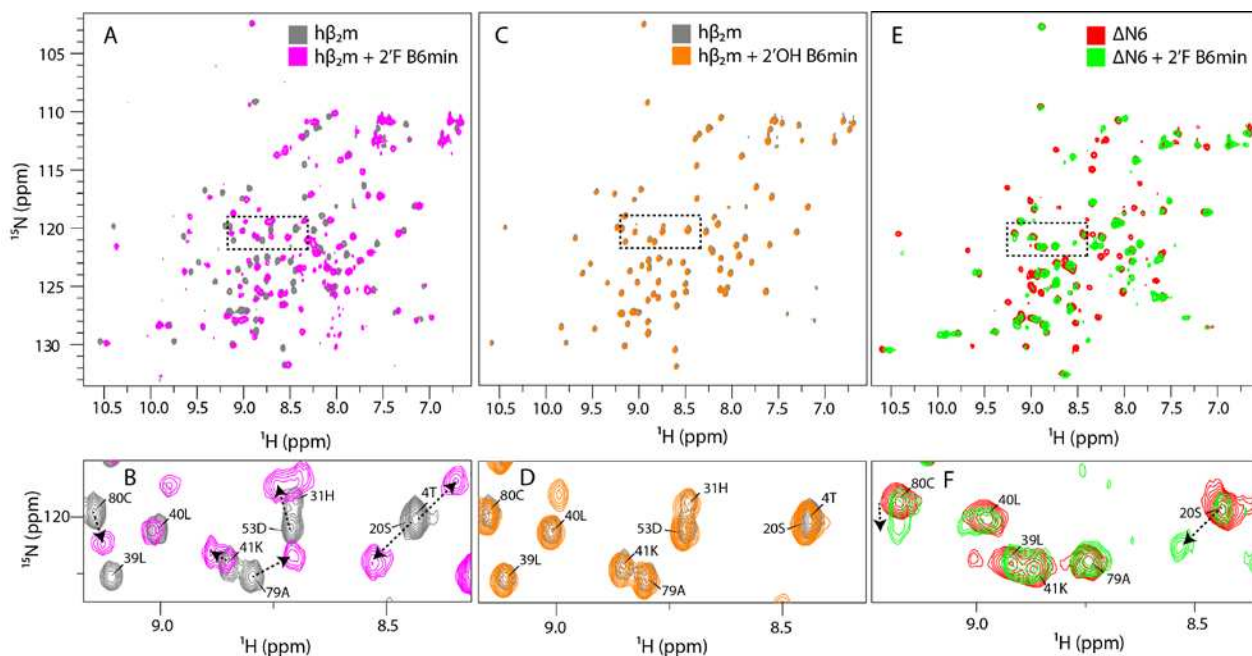


**Figure 5. Chemical shift changes upon the addition of aptamers to  $h\beta_2m$  and  $\Delta N6$ .** (A) The  $^1H$ - $^{15}N$  HSQC spectrum of  $^{15}N$ ,  $^{13}C$ -labeled  $h\beta_2m$  (60  $\mu M$ ) alone (grey) or in the presence of two molar equivalents of 2'F B6min (magenta). (B) Expansion of the region boxed in (A). (C) The  $^1H$ - $^{15}N$  HSQC spectrum of  $^{15}N$ ,  $^{13}C$ -labeled  $h\beta_2m$  (60  $\mu M$ ) alone (grey) or in the presence of two molar equivalents of 2'OH B6min (orange). (D) Expansion of the region boxed in (C). (E) The  $^1H$ - $^{15}N$  HSQC spectrum of  $^{15}N$ ,  $^{13}C$ -labeled  $\Delta N6$  (60  $\mu M$ ) alone (red) or in the presence of two molar equivalents of 2'F B6min (green). (F) Expansion of the region boxed in (E). Chemical shift changes in (B), (D) and (F) are annotated with arrows. All spectra were obtained at 25  $^{\circ}C$ , pH 6.2.



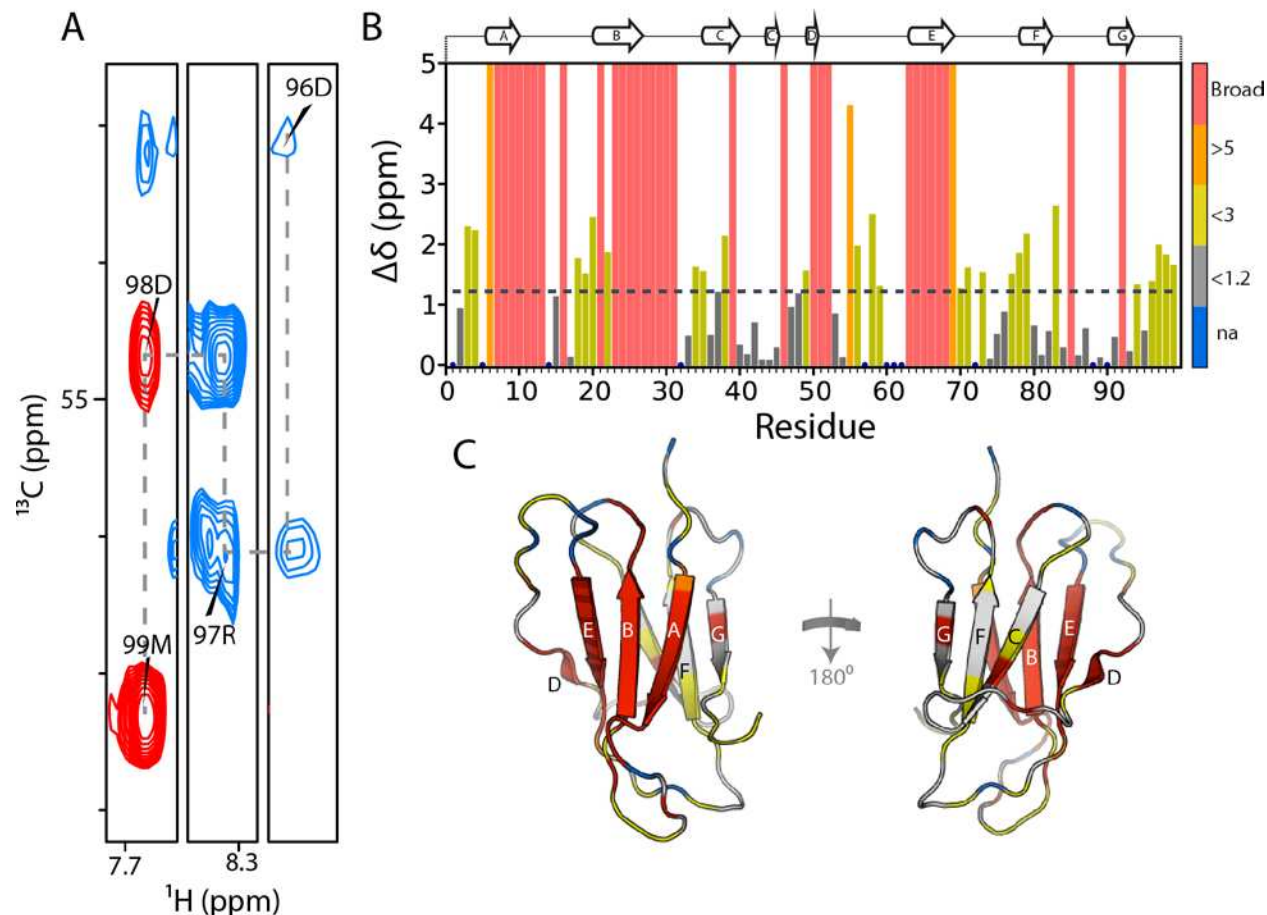


**Figure 6. Chemical shift changes upon binding of 2'F B6min to h $\beta_2$ m.** (A) Zoomed in regions of the 2D HNCA spectrum of  $^{13}\text{C}$ ,  $^{15}\text{N}$ -h $\beta_2$ m with 2 molar equivalents of 2'F B6min. The assignment walk on the  $\text{C}\alpha$ 's is shown for the four residues. (B) Chemical shifts changes of h $\beta_2$ m upon interaction with 2'F B6min. Total chemical shift change was calculated as  $\sqrt{(5^*H)^2 + (^{15}N)^2}$ . Residues for which assignments were not possible as a consequence of exchange broadening or large chemical shift perturbation are given an arbitrary value of 5 ppm and are shown in red. The dashed line represents two standard deviations of the mean over the entire data set. (C) The structure of h $\beta_2$ m coloured according to the measured chemical shift changes shown in (B).

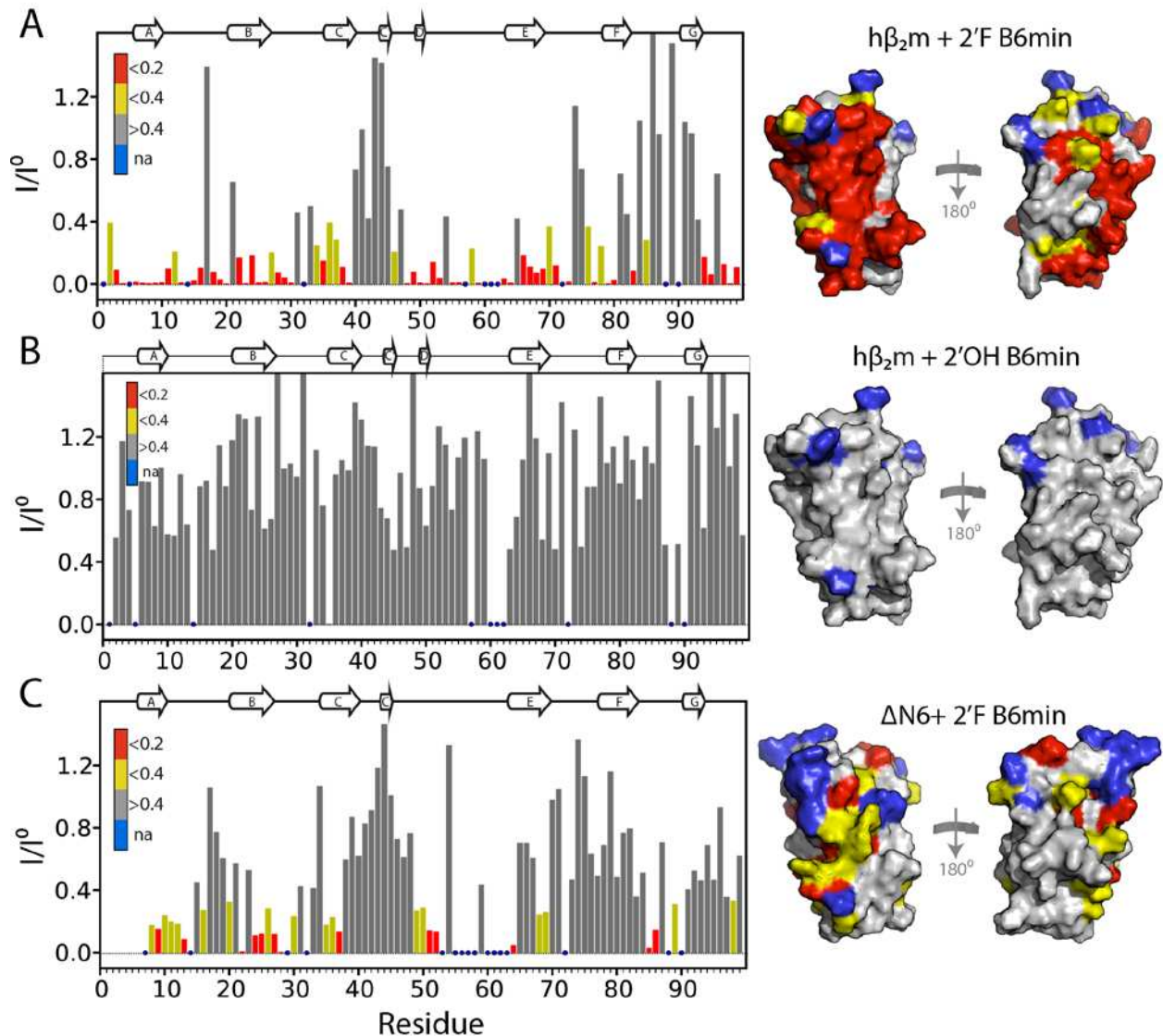


**Figure 7. 2'F B6 distinguishes between two highly similar proteins.** (A) Plot of the loss of signal intensity of resonances in native  $h\beta_2m$  upon binding to a 2-fold molar excess of 2'F B6min using data shown in Figure 5A. Profiles were calculated as the ratio of the peak intensity in the presence ( $I$ ) or absence ( $I^\circ$ ) of a 2-fold molar excess of aptamer. Intensity profiles were normalized to residues 40-45 that are not involved in the interface. Residues with a ratio of  $< 0.2$  are colored red, those showing a ratio between 0.2 and 0.4 are colored yellow, and those with no significant decrease in intensity are colored grey. The structure of  $h\beta_2m$  drawn as a surface representation is shown on the right color-coded using the same scale. Residues with no assignments (na) are shown in blue. (B) As in (A), but for the interaction of 2'OH B6min and  $h\beta_2m$ . (C) As in (A), but for the interaction of 2'F B6min with  $\Delta N6$ . The secondary structure elements of the proteins are show as ribbons on top of the panels.

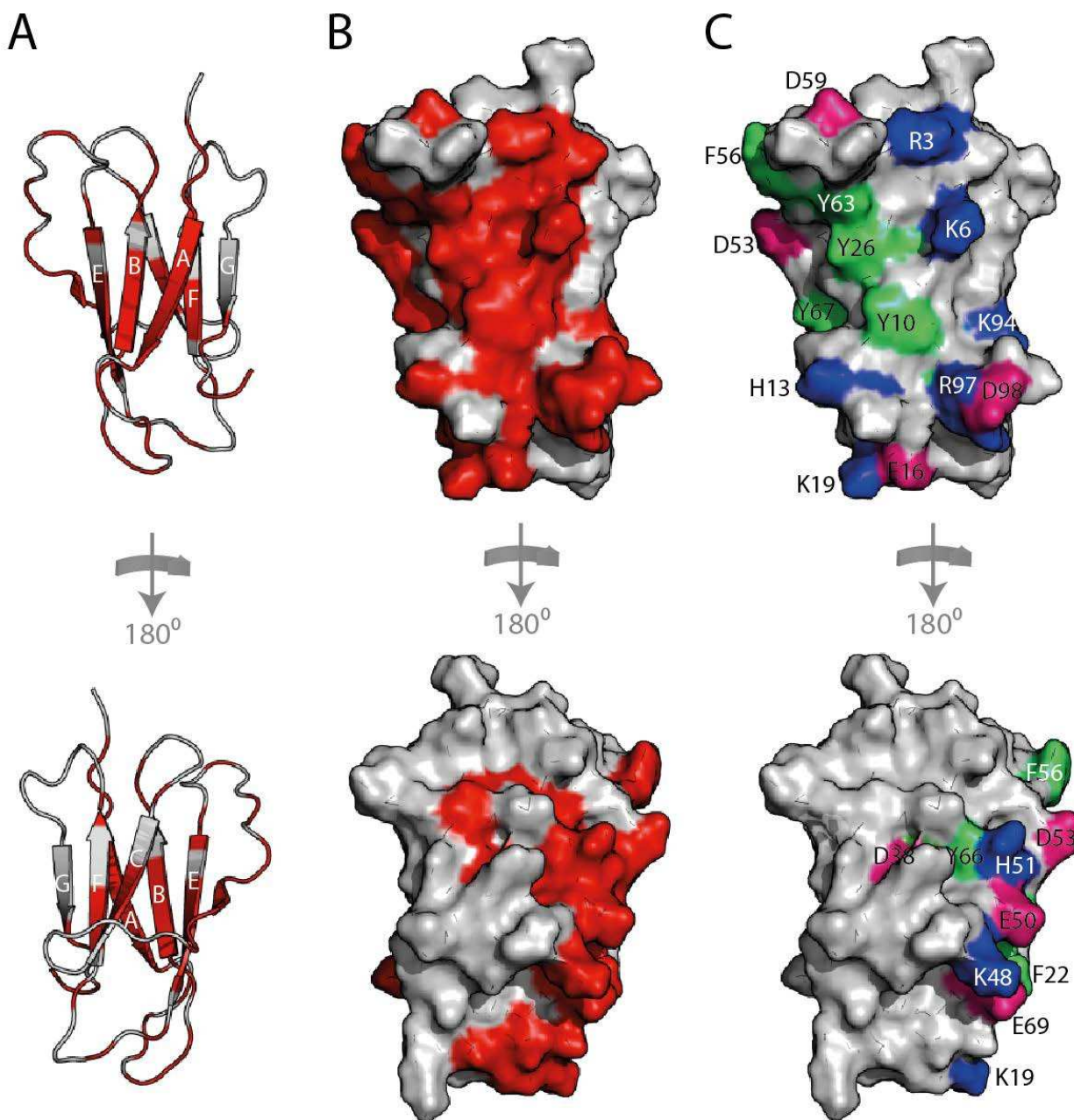


**Figure 8. Mapping the 2'F B6min-h $\beta_2$ m binding site.** (A) The residues in h $\beta_2$ m that show the largest decrease in intensity upon interaction with 2'F B6min are shown in red on the structure of h $\beta_2$ m (grey cartoon) and predominantly involve residues in the A, B, E, D  $\beta$ -strands of h $\beta_2$ m. By contrast, the C, F, G  $\beta$ -strands show relatively little change in intensity (bottom). (B) Surface representation of h $\beta_2$ m highlighting the interface residues (red). (C) The 2'F B6min-h $\beta_2$ m binding interface involves 7 aromatic residues (light green), 7 positively charged residues (blue) and 7 negatively charged residues (pink).

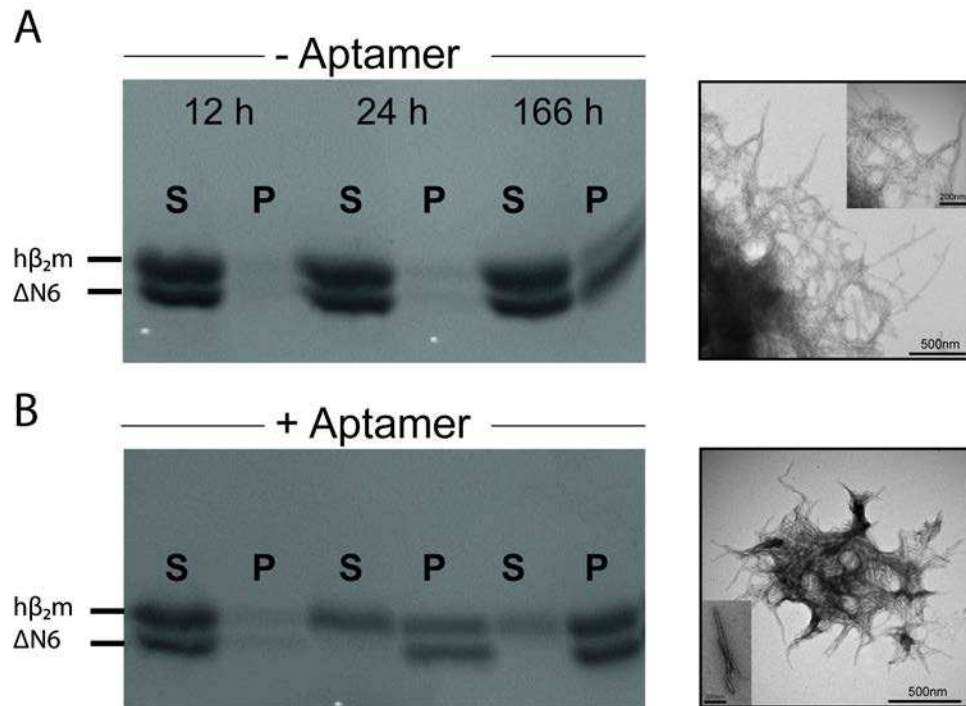


**Figure 9. 2'F B6min affects hβ<sub>2</sub>m-ΔN6 co-polymerization into fibrils.** (A) The course of aggregation of mixtures of hβ<sub>2</sub>m and ΔN6 (each 40 μM) in the absence of a 2-molar excess of aptamer determined by SDS PAGE. The morphology of the aggregates formed after 166 h is shown by TEM. (B), as for (A) but in the presence of a 2-fold molar excess of 2'F B6min. (S), supernatant; (P), pellet. Incubation was performed in 50 mM MES, 120 mM NaCl pH 6.2 with 600 rpm agitation at 37 °C. The scale bars on the TEM images represent 500 nm. For the inset TEM images the scale bars are 200 nm.



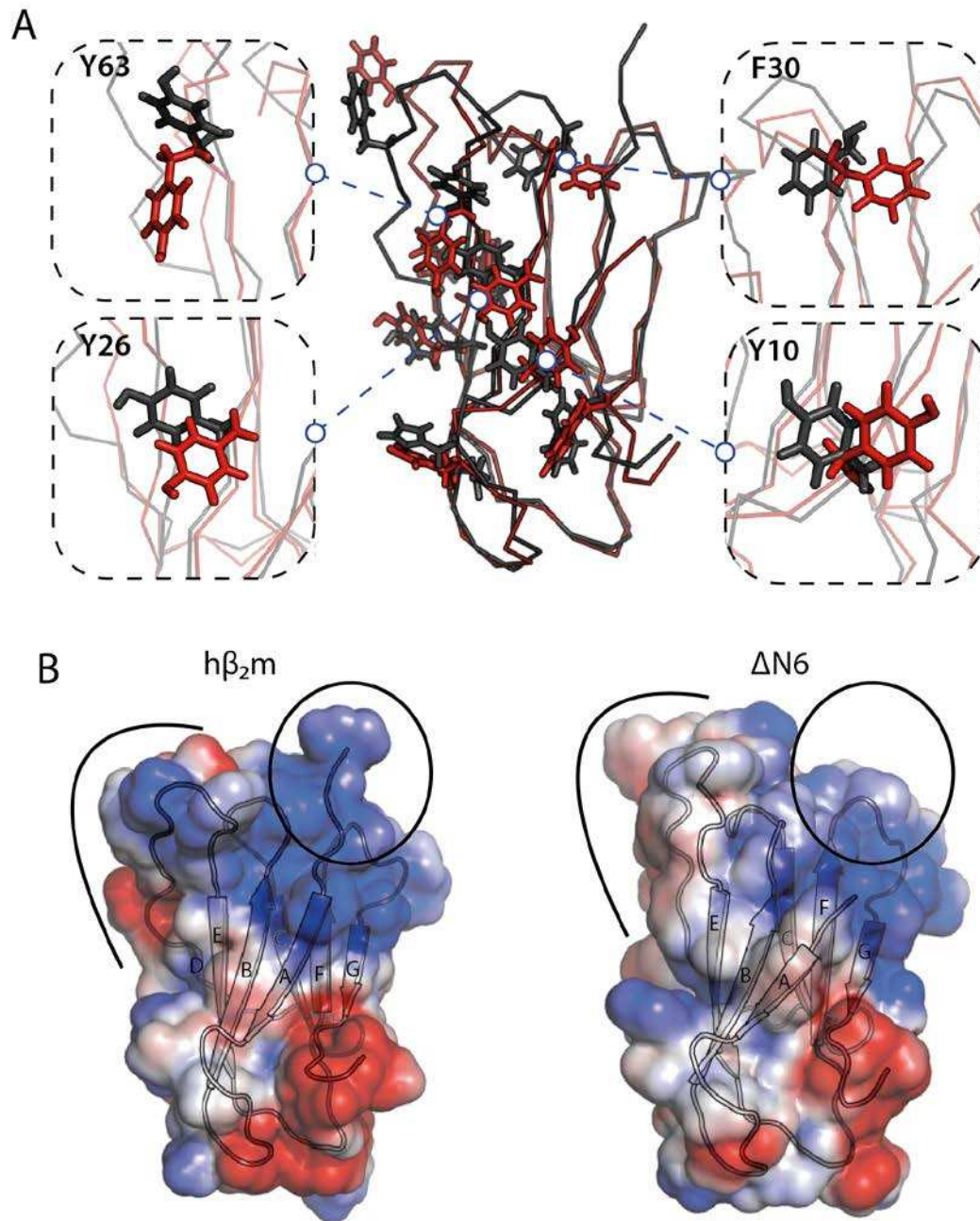


**Figure 10. Structural differences between hβ<sub>2</sub>m and ΔN6 in the aptamer binding surface.** (A) The aromatic residues located in the interface between 2' F B6min and hβ<sub>2</sub>m (see Figure 8) are highlighted as sticks on hβ<sub>2</sub>m (black ribbon) and ΔN6 (red ribbon). Zoom-in expansions of four residues are shown alongside. (B) The structure of hβ<sub>2</sub>m (left) and ΔN6 (right) shown as a surface representation colored by its electrostatic potential (blue positive, red negative). The N-terminal region is highlighted in a circle and the DE loop region is annotated with a black arc.



## **Distinguishing closely-related amyloid precursors using an RNA aptamer**

Claire J. Sarell, Theodoros K. Karamanos, Simon J. White, David H.J. Bunka, Arnout P. Kalverda, Gary S. Thompson, Amy M. Barker, Peter G. Stockley and Sheena E. Radford

*J. Biol. Chem.* published online August 6, 2014

---

Access the most updated version of this article at doi: [10.1074/jbc.M114.595066](https://doi.org/10.1074/jbc.M114.595066)

Alerts:

- [When this article is cited](#)
- [When a correction for this article is posted](#)

[Click here](#) to choose from all of JBC's e-mail alerts